1-1-1994

Ytterbium-Doped Apatite-Structure Crystals: A New Class Of Laser Materials

Stephen A. Payne

Laura D. DeLoach

Larry K. Smith

Wayne L. Kway

John B. Tassano

See next page for additional authors

Ytterbium-doped apatite-structure crystals: A new class of laser materials

Cite as: Journal of Applied Physics **76**, 497 (1994); https://doi.org/10.1063/1.357101
Submitted: 09 November 1993 . Accepted: 17 March 1994 . Published Online: 17 August 1998

Stephen A. Payne, Laura D. DeLoach, Larry K. Smith, Wayne L. Kway, John B. Tassano, William F. Krupke, Bruce H. T. Chai, and George Loutts

Ytterbium-doped apatite-structure crystals: A new class of laser materials

Stephen A. Payne, Laura D. DeLoach, Larry K. Smith, Wayne L. Kway, John B. Tassano, and William F. Krupke
Lawrence Livermore National Laboratory, University of California, P. O. Box 5508, Livermore, California 94550

Bruce H. T. Chai and George Loutts
Center for Research and Education in Optics and Lasers, University of Central Florida, Orlando, Florida 32826

(Received 9 November 1993; accepted for publication 17 March 1994)

A new class of Yb-lasers is summarized in this article. The apatite family of crystals, based on the hexagonal structure of the mineral fluorapatite, has been found to impose favorable spectroscopic and laser properties on the Yb^{3+} activator ion. Crystals of Yb-doped $Ca_5(PO_4)_3F$, $Sr_5(PO_4)_3F$, $Ca_xSr_{5-x}(PO_4)_3F$, and $Sr_5(VO_4)_3F$ have been grown and investigated. Several useful laser crystals have been identified which offer a variety of fundamental laser parameters for designing diode-pumped systems. In general, this class of materials is characterized by high emission cross sections ($3.6–13.1\times10^{-20}$ cm^2), useful emission lifetimes (0.59–1.26 ms), a strong pump band ($\sigma_{abs}=2.0–10.0\times10^{-20}$ cm^2), and pump and extraction wavelengths near 900 and 1045 nm, respectively. Efficient lasing has been demonstrated for several of the members of this class of materials, and high optical quality crystals have been grown by the Czochralski method. A summary of the laser parameters and a discussion of the Yb:apatite class of lasers is presented.

INTRODUCTION

Yb^{3+} has long been recognized to serve as a laser ion when incorporated as a dopant ion into $Y_3Al_5O_{12}$ and other garnets.[1] The main obstacle to further development entailed the limited pump absorption features that are available with Yb-doped crystals. Since Yb^{3+} is a $4f^{13}$ ion, it possesses only two relevant electronic states—the $^2F_{7/2}$ ground state and the $^2F_{5/2}$ excited state—separated by about 10 000 cm^{-1}. Since the prevailing pump sources in the 1960s and 1970s only included broad white light generating flash lamps, the single narrow absorption feature of Yb^{3+} proved to be an inadequate means of effectively pumping the laser material. While the need for a useful narrow band pump source was envisioned some time ago,[2] it was not until the emergence of InGaAs laser diodes that some workers recognized the renewed significance of Yb-doped materials.[3] In fact, with the availability of commercial laser diodes, the limited absorption features of Yb actually provide an advantage, since the lack of higher-lying excited states assures the absence of detrimental processes such as upconversion and excited state absorption. Additionally, the Yb^{3+} dopant offers an important advantage over the most common laser ion, Nd^{3+}, since its emission lifetime tends to be about four times greater when the same host medium is considered for both ions, thereby allowing for an enhanced level of energy storage.

The main complication associated with solid-state lasers based on the Yb ion involves the quasi-four-level nature of the system at room temperature. Otherwise stated, the problem is that the terminal laser level tends to reside at an energy of 200–600 cm^{-1}, which is comparable to the thermal energy present at room temperature (200 cm^{-1}).[3,4] Accordingly, the search for new Yb^{3+} lasers has been intimately tied to the structure of the energy levels and the strength of the transitions among them. In particular, the nature of the crystal field splitting in the $^2F_{7/2}$ and $^2F_{5/2}$ states and the cross section associated with the various $^2F_{7/2}$–$^2F_{5/2}$ transitions turns out to have a crucial impact on the viability of the system as a laser material. In brief, the ideal Yb laser would possess a high-lying crystal field component in the $^2F_{7/2}$ ground state, to which a particularly intense transition from the $^2F_{5/2}$ excited state would exist. The Yb-doped apatite class of laser materials to be described in this article is characterized by just such an energy level structure along with the desired transition strength moments.

As a result of our recent efforts, the Yb^{3+}-doped apatite-structure crystals may now potentially be employed in a variety of diode-pumped laser systems. This family of laser materials offers a substantial range of fundamental laser parameters with which systems may be designed, in order to adjust the pumping, storage, and energy extraction characteristics. In other words, the Yb-doped apatite class of materials allows a number of trade-offs, wherein the emission lifetime and cross section, as well as the pump linewidth and saturation parameters can be altered, albeit not independently of each other. A range of possibilities now exists such that the specific parameters of a given Yb:apatite laser medium can be matched to the requirements of a particular application.

The situation surrounding the Yb:apatite class of laser materials is not unlike the broadening of the scope of Nd:YAG ($Y_3Al_5O_{12}$) to encompass other oxide garnet hosts, such as $Gd_3Sc_2Ga_3O_{12}$ (GSGG), $Y_3Ga_5O_{12}$ (YGG), $Gd_3Ga_5O_{12}$ (GGG), and others. By way of illustration as to the type of property trade-offs that are encountered here, the Nd:GSGG crystal offers a wider pump band, larger crystals, and the potential for Cr^{3+} codoping, at the expense of reduced emission cross section, lower thermal conductivity, and melt instabilities associated with the gallium oxides.[5] In a similar manner, we began our campaign to identify new Yb lasers with the well-known mineral

 0021-8979/94/76(1)/497/7/$6.00

fluorapatite[6]—$Ca_5(PO_4)_3F$ or FAP— and then expanded our studies to other materials having the generic composition $A_5(MO_4)_3X$, where A=Ca, Sr, Ba; M=P, V; X=F, Cl. Among the many possible crystals having this formula, a few turned out to be useful Yb laser materials: $Sr_5(PO_4)_3F$ (S-FAP),[7] $Ca_3Sr_2(PO_4)_3F$ (C_3S_2-FAP),[8] and $Sr_5(VO_4)_3F$ (S-VAP). The point of this article is to describe the laser parameters and associated trade-offs encompassed within this new class of laser materials. It should be noted that FAP and S-FAP (also known as STRAP) were previously explored primarily as Nd-based laser media;[9,10] our contribution is to recognize that these particular host materials impose especially useful properties to the Yb^{3+} laser ion. It is noteworthy that Yb:YAG has proved to be the first highly effective diode-pumped laser material, as demonstrated and discussed in several recent articles,[11,12] and as originally suggested by Krupke and Chase.[3]

CRYSTAL GROWTH OF THE FLUOROPHOSPHATES AND FLUOROVANADATES

Although it has been reported that fluorapatite [$Ca_5(PO_4)_3F$ or FAP] melts congruently at 1700 °C, the actual melting process is complicated because the compound is composed of the two end members—calcium phosphate and calcium fluoride. As a result, the system may contain a congruently melting compound and an apatite solid solution of $Ca_9(PO_4)_6 \cdot xCaF_2$, where $x=0.88-1.0$. In our growth experiments, we did not observe the solid solution, but rather the continuous change of melt composition through evaporation and oxidation.

Initially we prepared the material based on the two-step reaction

$$9CaCO_3+6H_3PO_4 \rightarrow 3Ca_3(PO_4)_2+9CO_2+9H_2O),$$

and

$$3Ca_3(PO_4)_2+CaF_2 \rightarrow 2\,Ca_5(PO_4)_3F.$$

Because the reaction involves phosphoric acid in rather large quantities, the exact composition is difficult to control. An improved synthesis technique was therefore developed using the solid form of calcium hydrophosphate ($CaHPO_4$) as starting material so that the first reaction now becomes

$$6CaHPO_4+3CaCO_3 \rightarrow 3Ca_3(PO_4)_2+3CO_2+3H_2O.$$

While it is still necessary to use rare earth oxides and phosphoric acid to include rare earth dopants, the amount of acid used is much smaller and the system is far easier to handle.

Once the charge was made and melted, the crystals were grown by the Czochralski pulling method in a 3 in. Ir crucible. A two-loop weight feedback diameter control system was used in all the growth experiments. A neutral atmosphere is provided with a continuous flow of nitrogen. The typical growth rate is 1 mm/h while being rotated at 10–20 rpm. Up to 25% of the melt is converted to single crystal in about one week. Typical crystal size is 25 mm in diameter and 100 mm in length.

The growth technique for the strontium fluorapatite [$Sr_5(PO_4)_3F$ or S-FAP] is nearly identical to FAP although the growth temperature is much higher (1810 °C). We used strontium hydrogen phosphate ($SrHPO_4$) in the starting composition. The higher temperature causes heavier loss of the fluoride through evaporation. The fluorophosphates composed of the calcium-strontium mixtures exhibit behavior that is roughly intermediate to either of the end members.

As for the growth of strontium fluorovanadate [$Sr_5(VO_4)_3F$ or S-VAP], the technique is also similar. In this case we are able to use V_2O_5 powder as starting material and the synthesis reaction becomes

$$9SrCO_3+3V_2O_5 \rightarrow 3Sr_3(VO_4)_2+9CO_2,$$

and

$$3Sr_3(VO_4)_2+SrF_2 \rightarrow 2Sr_5(VO_4)_3F.$$

The melting temperature of S-VAP is lower (1650 °C) and the growth rate is higher (1.5 mm/h) than S-FAP.

The fluorapatite crystals may be described by the generic chemical formula $M_5(PO_4)_3F$, where the divalent metal ions, M, occupy two different crystallographic sites (referred to as I and II).[13] It has long been known, however, the trivalent rare earth dopants have a strong tendency to occupy the M_{II} site. This is the case because the fluoride ion resides in the coordination sphere and the charge compensation mechanism associated with rare earth doping involves the substitution of an oxide ion for the fluorine (viz., Ca^{2+}-F^- is replaced with Yb^{3+}-O^{2-}).[14,15] Although this simple situation is found to breakdown at high Yb doping levels it should adequately describe our crystals since their doping levels are rather low at $(3-10)\times10^{19}$ cm^{-3}.

SPECTROSCOPY

The room temperature absorption and emission properties of Yb-doped apatite crystals have been characterized. Absorption spectra were collected for oriented uniaxial crystals polarized both along the unique crystallographic c axis ($E \| c$), and perpendicular to the c axis ($E \perp c$). The spectra which were obtained on a Perkin Elmer Lambda 9 spectrometer were then converted to cross sections using the total Yb concentrations measured for each crystal by inductively coupled plasma and mass spectrometry. The Yb emissions were obtained by pumping each crystal with light from a Nd:YAG-pumped dye laser whose output is H_2 Raman shifted to yield pump wavelengths between 890 and 910 nm. The polarized emissions have been obtained using a grating monochromator and an S-1 photomultiplier tube for which the appropriate corrections have been applied to account for variations in the spectral response. The polarized emission spectra have also been converted to cross sections using the data analysis methods we have described in previous articles.[4,6] The upper level Yb lifetimes have been measured with the same pump/detector system using a transient digitizing oscilloscope to monitor the signal.

The measured absorption and emission cross sections, σ_{abs} and σ_{em}, and the upper level lifetimes, τ_{em}, can be used to assess several important laser performance parameters for different Yb:apatite lasers. In particular, β_{min}, which is defined as the minimum fraction of Yb ions that must be excited in order to balance the gain and the ground state absorption at the extraction wavelength, is crucial in quasi-

four-level systems such as Yb^{3+}. The β_{min} parameter may be determined then from the absorption and emission cross-section values for the extraction wavelength of the laser, λ_{ext}, according to

$$\beta_{min}=\frac{\sigma_{abs}(\lambda_{ext})}{\sigma_{abs}(\lambda_{ext})+\sigma_{em}(\lambda_{ext})}. \quad (1)$$

The β_{min} parameter may also be expressed in terms of the individual transitions between the crystal field components of the electronic states. In this case, from the known energies and degeneracies of the ground $^2F_{7/2}$ and the excited $^2F_{5/2}$ states, we can write:[6]

$$\beta_{min}=\left\{1+\frac{Z_l}{Z_u}\exp\left[\left(E_{ZL}-\frac{hc}{\lambda}\right)\Big/kT\right]\right\}^{-1}. \quad (2)$$

Here, Z_1 and Z_u are the partition functions of the ground and excited states, respectively, E_{ZL} is the "zero-line" energy separating the lowest crystal field components of the ground and excited states, and kT is a constant with a value of 205 cm^{-1} at room temperature.

Another performance parameter which can be assessed from the spectroscopic properties is the pump saturation intensity, I_{sat}. For efficient diode pumping, a large fraction of Yb ions must be excited in order to overcome the ground state absorption losses, and I_{sat} is a measure of the ease of bleaching the Yb-doped crystal. This pump parameter is assessed from the σ_{abs} value at the pump wavelength, λ_p, and the emission lifetime, τ_{em}, using

$$I_{sat}=\frac{hc}{\lambda_p\sigma_{abs}\tau_{em}}. \quad (3)$$

Clearly, higher absorption at the pump wavelength and longer Yb lifetimes are desirable for low values of I_{sat}.

Finally, an important parameter which takes into account both the absorption and emission characteristics of the Yb-laser crystal is I_{min}. In the case of lightly doped crystals, I_{min} is the minimum absorbed pump intensity which is required to reach threshold (in an otherwise lossless oscillator). This parameter is simply the product of our two previous laser performance indicators or

$$I_{min}=\beta_{min}I_{sat}. \quad (4)$$

For InGaAs diode laser pumping, output intensities from a two-dimensional array can be arranged to be of the order of 10 kW/cm^2, although it can be higher or lower depending on the nature of the diode array and the pump geometry. Lower values of I_{min} imply lower threshold lasers and therefore are more desirable when all else considered is equal.

The polarized absorption and emission cross sections of Yb:S-VAP are plotted for $E\|c$ and $E\perp c$ in Figs. 1 and 2, respectively. Interestingly, the uniaxial nature of the apatite structure has led to highly anisotropic, favorable spectral features. In particular, for light polarized along the c axis of the crystal, the absorption spectrum is dominated by a single, strong feature at 905 nm. Similarly, in the emission spectrum of $E\|c$, the oscillator strength is largely concentrated into the feature at 1044 nm. The high values of σ_{abs} and σ_{em} observed for these two peaks suggest useful pump and extraction parameters for a Yb:S-VAP laser.

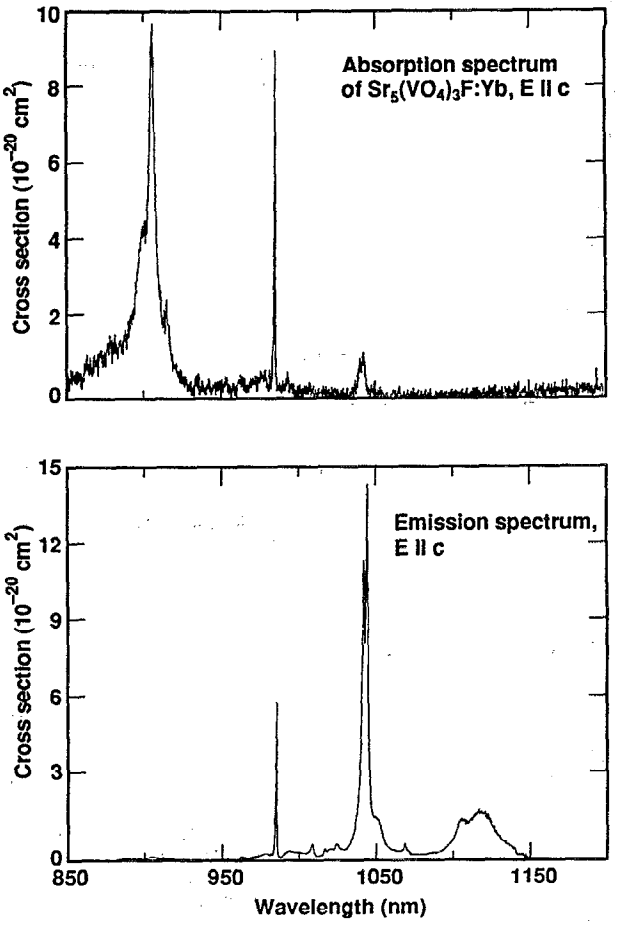

FIG. 1. Absorption and emission spectra of Yb in $Sr_5(VO_4)_3F$ (S-VAP), with $E\|c$, on absolute cross-section scale.

We have previously observed similar useful attributes in crystals of Yb:FAP[6] and Yb:S-FAP.[7] More recently, spectral determinations[8] have additionally been completed for several mixed crystals of $Ca_{5-x}Sr_x(PO_4)_3F$:Yb. For comparison, the absorption and emission spectra are compiled into composite figures each with $Ca_5(PO_4)_3F$, $Ca_4Sr(PO_4)_3F$, $Ca_3Sr_2(PO_4)_3F$, $Ca_2Sr_3(PO_4)_3F$, and $Sr_5(PO_4)_3F$, shown plotted for $E\|c$ on an absolute cross section scale in Figs. 3 and 4. The important measured spectral properties (cross sections, linewidths, and lifetime) of σ_{abs}, σ_{em}, $\Delta\lambda_{abs}$, $\Delta\lambda_{em}$, and τ_{em} are also summarized in Table I for all of these Yb:apatites together with the calculated parameters of β_{min} and I_{min}. It turns out that the main absorption and emission features are strongly π polarized for all of the Yb-doped apatites studied thus far.

Figures 1–4 and Table I reveal the similar Yb spectroscopy arising from the apatite-structure crystals, but also show significant variations among the properties. It is noteworthy, for example, that the prominent absorption and emission cross-section peaks decrease among the mixed Ca,Sr apatites and that their bandwidths accordingly increase. For diode pumping of Yb:apatite lasers, of course, the pump bandwidth is an important parameter, with greater bandwidths giving some advantages in terms of a relaxed wavelength specification on the laser diode pump. The decrease in

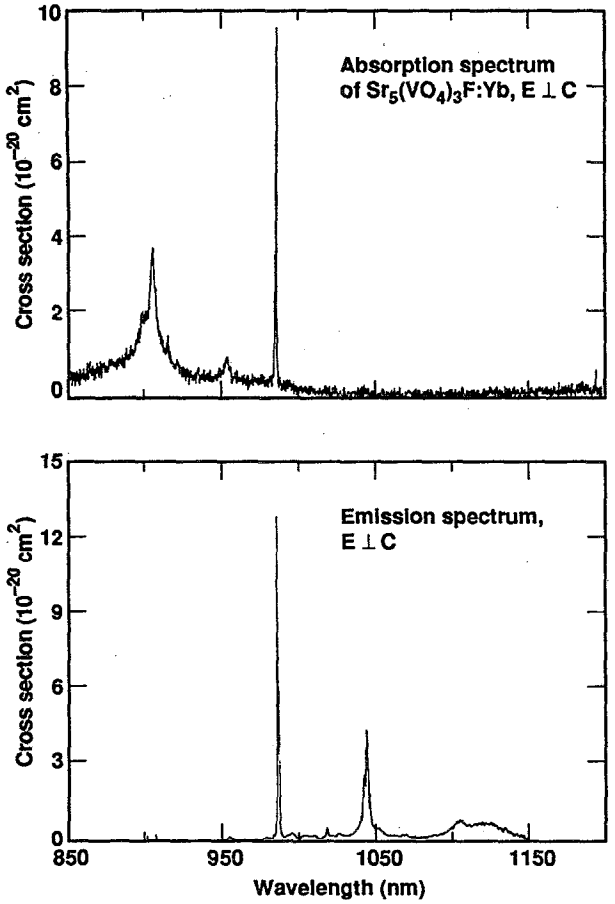

FIG. 2. Absorption and emission spectra of Yb:$Sr_5(VO_4)_3F$ with $E \perp c$.

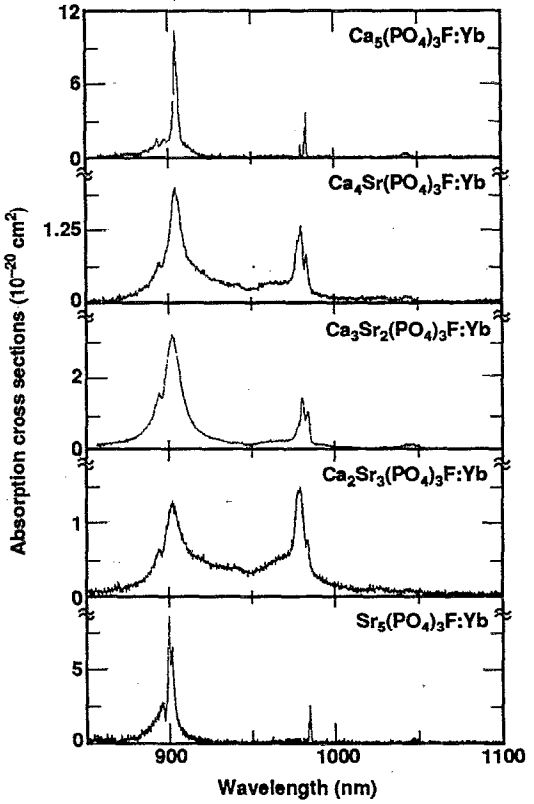

FIG. 3. Absorption spectra of Yb in the series of crystals $Ca_{5-X}Sr_X(PO_4)_3F$, where $X=0$, 1, 2, 3, and 5. Spectra are plotted on an absolute cross-section scale and shown for $E \| c$. Notice the broadening of the features in the mixed hosts.

absorption and emission cross sections, although still comparatively high among Yb-doped materials, leads to somewhat inferior values for $I_{\min}$. In comparison, although the Yb-doped S-VAP crystal has high cross sections and greater bandwidths than observed in the end-member fluorophosphates, it also is characterized by a reduced Yb lifetime. Nevertheless, $I_{\min}$, although larger than in FAP and S-FAP, is still reasonably small for Yb:S-VAP. Note that the Yb ions appear to occupy a second kind of site in the $Ca_2Sr_3(PO_4)_3F$ host, and that this crystal is probably not useful for laser applications.

As a useful way to compare the potential laser performance of known Yb-doped apatite crystals, we display data points on a figure-of-merit plot with σ_{em} on the ordinate and $I_{\min}$ on the abscissa. Such a plot is presented in Fig. 5 and includes the data points of several Yb-doped crystals which we have presented in an earlier article.[4] This plot very clearly demonstrates that the favorable high σ_{em}, low $I_{\min}$ space is uniquely occupied by the various apatite structure crystals we have been investigating.

LASER PERFORMANCE

The cw laser performance was assessed for all but one of the crystals that were spectroscopically characterized in the last section. Here we present data to prove that the Ca-Sr mixed apatite crystals, as well as the new fluorovanadate host, serve as useful laser media. Furthermore, the prior results obtained for Yb:FAP[6] and Yb:S-FAP[7] will be briefly reviewed. Overall, four new Yb-based laser crystals have been recognized to lase effectively.

Since we have already described the techniques employed to measure the laser efficiencies,[6,7] only the highlights of our methods will be outlined here. The Yb-doped crystals were cut to 0.5–1.0 cm in length with parallel uncoated windows, and were arranged to be at the center of a 10-cm-long concentric cavity. The Ti:sapphire pump laser output was set to 900–905 nm, and chopped to a duty cycle of 25% before impinging on the crystal (although operating in the true cw mode appeared to have little or no impact on the Yb-laser output). One of the subtle issues encountered involved correctly evaluating the absorbed fraction of pump light since the Yb^{3+} ions tend to bleach at the typical pump levels employed; this situation is illustrated for the lower curve in Fig. 6 for the $Ca_5(PO_4)_3F$:Yb system. We must recall, however, that the inversion density (and therefore the extent of bleaching) becomes *clamped*[16] at the magnitude present at the threshold of laser operation. It is necessary, therefore, to determine the absorbed fraction while the Yb laser is actually operating. As described in detail in Ref. 6, this is accomplished using the relationship

$$1-F_1=(1-F_{nl})(P_l/P_{nl}), \tag{5}$$

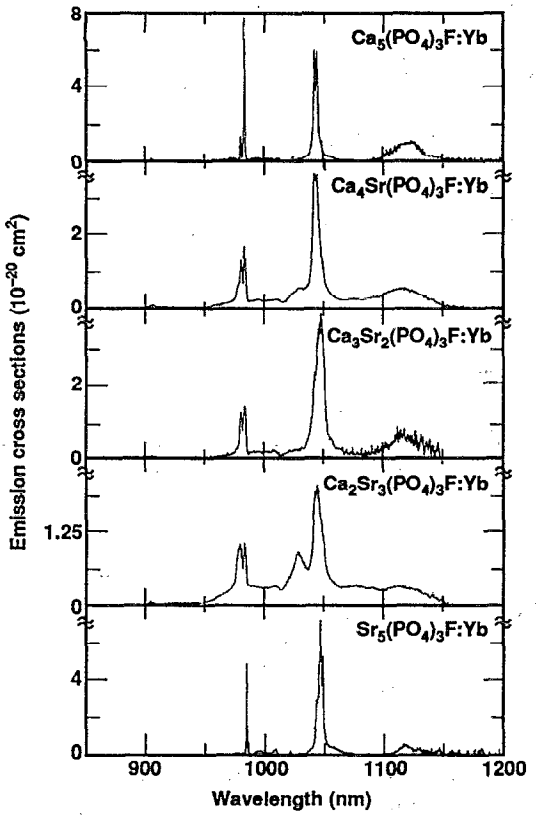

FIG. 4. Emission spectra of Yb:$Ca_{5-x}Sr_x(PO_4)_3F$ with $E\|c$.

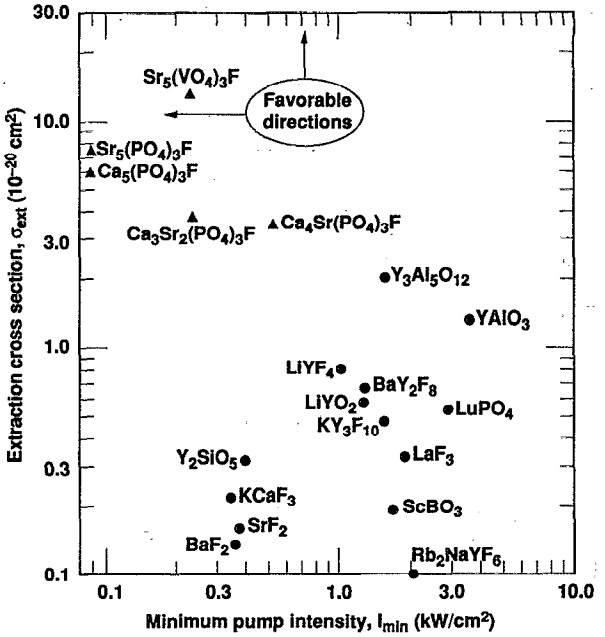

FIG. 5. Plot of the extraction cross section (σ_{ext}) against the minimum absorbed pump intensity required to yield net gain (I_{min}). All of the Yb-doped apatite-structure crystals are located in the superior upper-left-hand sector of this plot.

where F_l and F_{nl} are the fractions of pump light absorbed with the laser operating and when laser action is spoiled, respectively, and P_l/P_{nl} is a relative measure of the pump light leaking through the output coupler with/without the Yb-laser operating. After applying the P_l/P_{nl} correction of Eq. (5), the upper curve of Fig. 6 is obtained, where it is seen that, at the threshold of about 50 mW (at the curve crossing), the inversion is clamped and the absorbed fraction becomes fixed at F_l=0.80 while F_{nl} continues to drop to a level as low as 0.2. The data in Fig. 6 are a clear experimental illustration of one of the most basic tenets in laser physics.

Using the experimental approach outlined above, we have produced laser action in Yb:S-VAP [$Sr_5(VO_4)_3F$], Yb:C_4S-FAP [$Ca_4Sr(PO_4)_3F$], and Yb:C_3S_2-FAP [$Ca_3Sr_2(PO_4)_3F$]. Several examples of the laser data obtained for Yb:S-VAP are displayed in Fig. 7, where the output couplings employed ranged from 4.4% to 19.8%, yielding slope efficiencies of 36.6%, 56.4%, and 62.9%, with respect to the absorbed pump power. Several additional plots of the output power versus absorbed pump power appear in Fig. 8, including Yb in both of the mixed apatite hosts, C_3S_2-FAP and C_4S-FAP, operating near the standard 1046 nm wavelength. Interestingly, we were able to also lase the Yb:C_4S-FAP crystal at 1110 nm, which corresponds to the longer wavelength, weaker emission band shown in Fig. 4. We expect that all of the Yb-doped apatite crystals are amenable to laser action at this longer wavelength. It is noteworthy that, in spite of the low cross-section value, the generation of 1110 nm output is somewhat enhanced by the fact that true four-level operation is possible at this wavelength (i.e., no ground state absorption is present).

The summary of the slope efficiencies and thresholds obtained for the aforementioned crystals and wavelengths is listed in Table II, where averages over two runs are sometimes reported. Note that Yb:C_4S-FAP has also been demonstrated to lase at 985 nm (with $E\perp c$). Since this spectral line corresponds to the transition between the lowest crystal field components of the $^2F_{7/2}$ ground and $^2F_{5/2}$ excited states, these experiments correspond to true three-level operation of

TABLE I. Spectroscopic properties of Yb-doped apatite crystals for 1043–1047 nm laser action.

Host	σ_{abs} (10^{-20} cm^2)	$\Delta\lambda_{abs}$ (nm)	τ_{em} (ms)	σ_{em} (10^{-20} cm^2)	$\Delta\lambda_{em}$ (nm)	β_{min} (kW/cm^2)	I_{min}
$Sr_5(VO_4)_3F$	7.5	4.0	.59	13.1	4.7	0.047	0.23
$Ca_5(PO_4)_3F$	10.0	2.4	1.08	5.9	4.1	0.047	0.09
$Ca_4Sr(PO_4)_3F$	2.0	10.0	0.90	3.6	7.2	0.044	0.53
$Ca_3Sr_2(PO_4)_3F$	3.8	11.8	1.06	3.8	9.6	0.042	0.23
$Sr_5(PO_4)_3F$	8.6	3.7	1.26	7.3	4.0	0.043	0.09

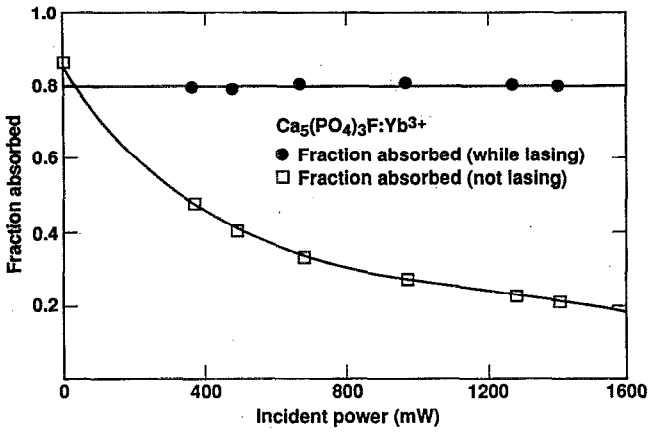

FIG. 6. Absorbed fraction of pump light as a function of incident power at 905 nm, for the case of operating Yb laser, and for simple single-pass absorption.

this system. Therefore the 985, 1046, and 1110 nm operating wavelengths of Yb:C_4S-FAP in Table II correspond to three, quasi-four, and four-level operation of the laser!

The data of Table II can be processed further on the basis of the plotting technique proposed by Caird.[17] This technique requires that the simple equation describing the slope efficiency, η, in the limit of low (double-pass) loss, L_d, and low output coupling, T

$$\eta = \eta_0 \frac{T}{T+L}, \tag{6}$$

be inverted to yield

$$\eta^{-1} = \eta_0^{-1} + \left(\frac{L}{\eta_0}\right) T^{-1}. \tag{7}$$

Here the intercept with the ordinate, η_0, provides a measure of the so-called intrinsic efficiency. η_0 is simply given by the ratio of the pump and laser wavelengths, or about 86% for the Yb:apatite crystal family. The application of Eq. (7) to the Yb:S-VAP laser data is illustrated in Fig. 9, where the derived η_0 value of 83% is found to be remarkably close to the quantum defect limited value of 86%. The double-pass loss of L_d=5.9% suggests that parasitic absorption and/or scattering may be issues for these new materials at this time. The existence of passive loss during the early stages in the development of any new material is, of course, a common problem.[18]

A summary of the single-pass losses and intrinsic efficiencies obtained for all of the Yb:apatite laser crystals is summarized in Table III, where η_0 values of 65%–84% are all in accord with the imposed fundamental quantum limit of 86%—the tendency to not attain the theoretical maximum is most likely a consequence of inadequate mode matching of the pump and cavity fields. The variation of the single-pass

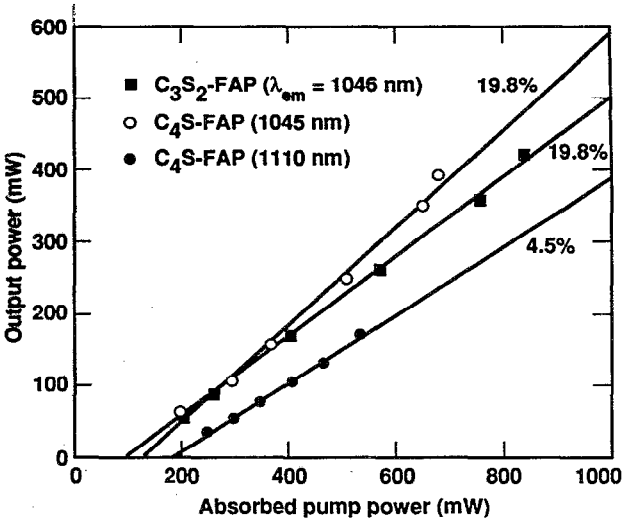

FIG. 8. Illustrative laser efficiency results obtained for the mixed apatites, including Yb:C_3S_2-FAP at 1046 nm, and Yb:C_4S-FAP at 1045, 1110, and 985 nm. The output coupling values are explicitly noted in the figure; the slope efficiencies are reported in Table II; the derived intrinsic efficiencies and double-pass loss values are listed in Table III.

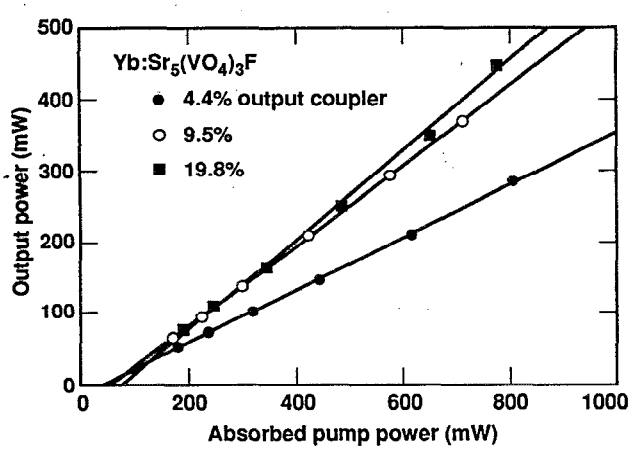

FIG. 7. Laser efficiency data acquired for Yb:S-VAP for the three indicated output coupler values at 1044 nm with $E \| c$.

TABLE II. Slope efficiency and threshold values for several Yb-doped crystals (averaged over several runs).

Crystal	Output coupling (%)	Wavelength (nm)	Slope efficiency (%)	Threshold (mW)
S-VAP	4.4	1044	35.2	46
	9.5	1044	56.4	52
	19.8	1044	61.4	69
C_4S-FAP	4.4	1046	44.5	76
	9.5	1046	54.6	88
	19.8	1046	67.1	123
	0.8	1110	15.2	186
	3.1	1110	40.6	135
	4.5	1110	44.4	169
	1.6	985	5.5	516
C_3S_2-FAP	2.5	1046	26.3	103
	4.4	1046	35.3	75
	9.5	1046	46.8	83
	19.8	1046	55.2	112

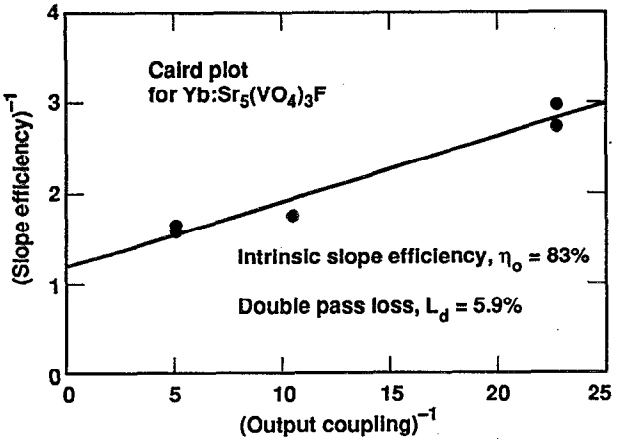

FIG. 9. Caird plot for Yb:S-VAP using the measured slope efficiencies obtained at 1044 nm for the individual laser output runs. The derived intrinsic efficiency and double-pass loss are noted.

loss from 0.7% to 3.0% is the result of variation in the quality of optical materials that have been employed. On the basis of the data presented in this section, the laser performance of the Yb-doped apatite crystals is judged to be good at this time, and may be expected to improve further as lower loss material becomes available. Finally, it is mentioned for completeness that the thermomechanical properties of these crystals have been previously discussed in Refs. 4, 7, and 19. In brief, they are less robust than hosts such as YAG, and are similar to other common crystals like YLF. Interestingly, since the change of refractive index with temperature dn/dT is negative for all the apatites considered here, the thermal lens is likely to be reduced somewhat.

CONCLUSION

We have defined a new class of laser media based on the Yb^{3+} ion that offers a substantial range of laser parameters. The emission cross section was found to be as low as 3.6×10^{-20} cm^2 for Yb in the $Ca_4Sr(PO_4)_3F$ (C_4S-FAP) host, and as large as 13.1×10^{-20} cm^2 for Yb:$Sr_5(VO_4)_3F$ (S-VAP). The emission cross-section variations are, of course, directly tied to changes in the emission lifetime (0.59–1.26 ms). Importantly, the mixed crystals of Yb in C_4S-FAP and C_3S_2-FAP offer substantially enhanced pump bandwidths that are on the order of 10–12 nm (FWHM), thereby relaxing the wavelength specification requirement that must be imposed on the diode laser pump source. On the other hand, Yb:FAP and Yb:S-FAP are expected to exhibit the lowest possible thresholds among the Yb:apatite family of materials. All of the crystals have been demonstrated to lase efficiently and can be grown as high-quality optical materials by the Czochralski method. We believe that the Yb:apatite class of lasers is useful for low- and medium-power applications, and will be preferred over the more common Nd lasers in many situations by virtue of their longer lifetime.

TABLE III. Summary of laser efficiency analysis for Yb-doped apatite crystals.

Crystal	Wavelength (nm)	Intrinsic efficiency (%)	Single-pass loss (%)	Path length (cm)
S-VAP	1044	83	3.0	0.57
FAP[a]	1043	84	1.2	0.69
C_4S-FAP	1046	76	1.7	0.75
	1110	81	2.7	
C_3S_2-FAP	1046	65	1.8	0.65
S-FAP[b]	1047	70	0.7	0.70

[a]Reference 6.
[b]Reference 7.

ACKNOWLEDGMENTS

We wish to thank Charles Otto and Theresa Duewer for providing chemical analyses of the samples investigated. We thank Eberhard Prochnow and Ron Vallene for expert fabrication and finishing of the crystals used in the optical studies. This work was performed under the auspices of the U.S. Department of Energy by Lawrence Livermore National Laboratory under Contract No. W-7405-ENG-48.

[1] G. A. Bogomolova, D. N. Vylegzhanin, A. A. Kaminskii, Sov. Phys. JETP **42**, 440 (1976).
[2] A. R. Reinberg, L. A. Riseberg, R. M. Brown, R. W. Wacker, and W. C. Holton, Appl. Phys. Lett. **19**, 11 (1971).
[3] W. F. Krupke and L. L. Chase, Opt. Quantum Electron. **22**, S1 (1990).
[4] L. D. DeLoach, S. A. Payne, L. L. Chase, L. K. Smith, W. L. Kway, and W. F. Krupke, IEEE J. Quantum Electron. **QE-29**, 1179 (1993).
[5] W. F. Krupke, M. D. Shinn, J. E. Marion, J. A. Caird, and S. E. Stokowski, J. Opt. Soc. Am. B **3**, 102 (1986).
[6] S. A. Payne, L. K. Smith, L. D. DeLoach, W. L. Kway, J. B. Tassano, and W. F. Krupke, IEEE J. Quantum Electron. **QE-30**, 170 (1994); R. Scheps, J. F. Myers, and S. A. Payne, IEEE Photon Technol. Lett. **5**, 1285 (1993).
[7] L. D. DeLoach, S. A. Payne, L. K. Smith, W. L. Kway, and W. F. Krupke, J. Opt. Soc. Am. B **11**, 269 (1994).
[8] L. D. DeLoach, S. A. Payne, B. H. T. Chai, W. F. Krupke, L. K. Smith, W. L. Kway, and J. B. Tassano, *OSA Proceedings on Advanced Solid-State Lasers*, edited by A. A. Pinto and T. Y. Fan (Optical Society of America, Washington, DC, 1993), pp. 188–191.
[9] K. B. Steinbruegge, T. Henningsen, R. H. Hopkins, R. Mazelsky, N. T. Melamed, E. P. Reidel, and G. W. Roland, Appl. Opt. **11**, 999 (1972).
[10] R. Mazelsky, R. H. Hopkins, and W. E. Kramer, J. Cryst. Growth **34**, 260 (1969).
[11] P. Lacovara, H. K. Choi, C. A. Wang, R. L. Aggarwal, and T. Y. Fan, Opt. Lett. **6**, 1089 (1991).
[12] T. Y. Fan, IEEE J. Quant. Electron. **QE-28**, 2692 (1992).
[13] S. Naray-Szabo, Z. Krist **75**, 387 (1930).
[14] A. A. Kaplyanskii and E. G. Kuzminov, Opt. Spectrosc. **29**, 376 (1970).
[15] F. M. Ryan, R. W. Warren, R. H. Hopkins, and J. Murphy, J. Electrochem. Soc. **125**, 1493 (1978).
[16] A. Yariv, *Quantum Electronics* (Wiley, New York, 1975).
[17] J. A. Caird, S. A. Payne, P. R. Staver, A. J. Ramponi, L. L. Chase, and W. F. Krupke, IEEE J. Quantum Electron. **QE-24**, 1077 (1988).
[18] P. R. Moulton, J. Optical Soc. Am. B **3**, 125 (1986).
[19] B. H. T. Chai, G. Loutts, X. X. Zhang, S. A. Payne, W. F. Krupke, L. D. Deloach, and L. K. Smith, Opt. Lett. (to be published).